
SenseShift6D: Multimodal RGB-D Benchmarking for Robust 6D Pose Estimation across Environment and Sensor Variations

Yegyu Han¹ Taegyeon Yoon¹ Dayeon Woo¹ Sojeong Kim² Hyung-Sin Kim¹

¹Graduate School of Data Science, Seoul National University

²Department of EECS, Gwangju Institute of Science and Technology

{yegyuhan, taegyoun88, wuvel22}@snu.ac.kr, kimsojeong@gm.gist.ac.kr
hyungkim@snu.ac.kr

Abstract

Recent advances on 6D object-pose estimation has achieved high performance on representative benchmarks such as LM-O, YCB-V, and T-Less. However, these datasets were captured under fixed illumination and camera settings, leaving the impact of real-world variations in illumination, exposure, gain or depth-sensor mode – and the potential of test-time sensor control to mitigate such variations – largely unexplored. To bridge this gap, we introduce *SenseShift6D*, the first RGB-D dataset that physically sweeps 13 RGB exposures, 9 RGB gains, auto-exposure, 4 depth-capture modes, and 5 illumination levels. For three common household objects (spray, pringles, and tincase), we acquire 101.9k RGB and 10k depth images, which can provide 1,380 unique sensor-lighting permutations per object pose. Experiments with state-of-the-art models on our dataset show that applying sensor control during test-time induces greater performance improvement over digital data augmentation, achieving performance comparable to or better than costly increases in real-world training data quantity and diversity. Adapting either RGB or depth sensors individually is effective, while jointly adapting multimodal RGB-D configurations yields even greater improvements. *SenseShift6D* extends the 6D-pose evaluation paradigm from data-centered to sensor-aware robustness, laying a foundation for adaptive, self-tuning perception systems capable of operating robustly in uncertain real-world environments.

Our dataset is available at: huggingface.co/datasets/Yegyu/SenseShift6D

Associated scripts can be found at: github.com/yegyu-han/SenseShift6D

1 Introduction

Estimating the 6D pose of everyday objects is a critical computer vision task, enabling fine-grained interactions in mixed-reality headsets, autonomous-vehicle manipulation, and embodied AI agents navigating cluttered environments [5, 28, 24, 26, 16, 21]. The field has made substantial progress, with state-of-the-art methods achieving high accuracy on established benchmarks [7, 3, 10, 15, 11].

However, these impressive results are achieved under strictly controlled acquisition settings. Real-world deployments, in contrast, face variations: ambient illumination changes throughout the day, camera exposure and gain settings are adjusted by on-board auto-control or user preference, and commodity depth sensors can also switch capture modes on purpose. These environmental and sensor dynamics introduce complex artifacts, including nonlinear color shifts and structured depth noise, which are challenging to replicate accurately with synthetic augmentations or compensate for during post-processing [1]. Consequently, existing benchmarks – collected with fixed illumination, exposure, gain, and depth configurations – cannot adequately represent real-world scenarios. Therefore, the research community lacks a systematic benchmark for quantifying how 6D-pose estimators respond

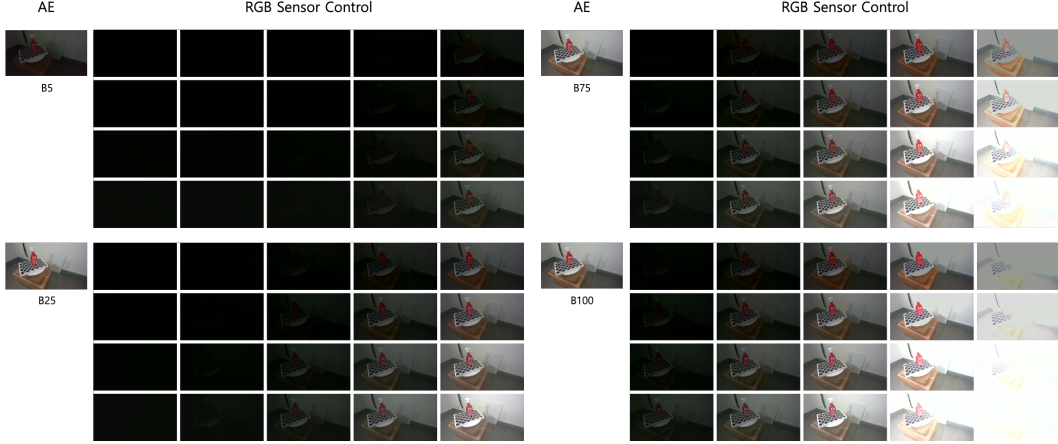


Figure 1: RGB sample images under auto exposure and under all combinations of exposure and gain settings for brightness 5%, 25%, 75% and 100%. Rows indicate gain levels and columns indicate exposure levels.

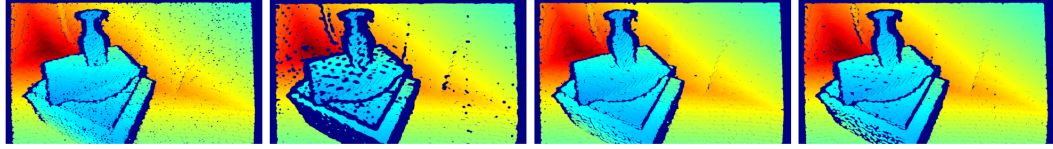


Figure 2: Depth sample images under four depth capture modes: default, high accuracy, high density, and medium density.

to per-frame sensor variation or for evaluating emerging test-time sensor-control strategies [1, 2] designed to mitigate these shifts.

Recent attempts to tackle this robustness gap have explored adaptive sensor control, which dynamically adjusts sensor parameters at test time to maximize accuracy without modifying the underlying model. Studies in image classification have demonstrated that test-time sensor control improves model robustness more effectively than scaling up the model size or augmenting training data [1, 2]. However, these efforts have been limited to unimodal RGB tasks. Importantly, no prior work has examined multimodal (RGB and depth) sensor control or provided a benchmark that physical sweeps multimodal sensor parameters with ground-truth 6D pose. Consequently, the effectiveness of adaptive multimodal sensing and its interplay with traditional data-centric training remain an open question.

To bridge this gap, we introduce *SenseShift6D*, a novel RGB-D benchmark for 6D pose estimation that physically sweeps key sensor and lighting parameters. Using an Intel RealSense RGB-D camera in a controlled darkroom setup, we systematically vary 13 exposure levels, 9 gain settings, 4 depth-capture modes, and 5 illumination conditions across three representative household objects: a textured spray can, a cylindrical Pringles tube, and a glossy tin case. This protocol produces a dataset of 101.9k RGB and 10k depth frames, which can provide 1,380 unique sensor-lighting permutations per object pose (as illustrated in Figures 1 and 2), each annotated via 6D ground-truth via ArUco calibration and manual refinement (with ~ 3 mm errors). For controlled study, experiments in this paper are conducted on the four subsets of the entire dataset: **Train-Def**, recorded under default camera and illumination settings, and **Train-Var**, covering a comprehensive multimodal parameter grid (8 exposure, 5 gain, auto-exposure, 4 depth-capture settings with 5 lighting conditions). Correspondingly, we construct two test splits (**Test-Def** and **Test-Var**) without overlap with the training configurations. As all variations are physically realized, the captured images preserve authentic sensor artifacts, including nonlinear color shifts, photon-shot noise, and structured depth errors, that synthetic augmentations cannot replicate. Thus, *SenseShift6D* establishes the first realistic testbed for sensor-aware 6D pose estimation and adaptive sensing.

This paper offers three main contributions:

- **Sensor-aware multimodal benchmarking:** We present the first 6D object-pose benchmark that systematically and physically varies multimodal sensor parameters across frames, enabling fine-grained analysis of sensor-dependent performance degradation.

Table 1: Comparison of 6D pose estimation datasets in terms of sensor and lighting variation.

Dataset	Environmental and sensor variations				Objects	RGB frames	Depth frames
	Illumination	Exposure	Gain	Depth			
LM (ACCV '12) [7]	×	×	×	×	15	18.2k	18.2k
LM-O (ECCV '14) [3]	×	×	×	×	8	1.2k	1.2k
T-LESS (WACV '17) [10]	×	×	×	×	30	49k	49k
YCB-V (RSS '18) [27]	×	×	×	×	21	133k	133k
TUD-L (ECCV '18) [11]	8 locations	×	×	×	3	62k	62k
HB (ICCVW '19) [15]	2 locations	×	×	×	33	34.8k	34.8k
HOPE (IROS '22) [23]	5 locations	×	×	×	28	238	238
IPD (CVPR '24) [14]	3 locations	4 levels	×	×	20	30k	30k
SenseShift6D (Ours)	5 levels	13 levels	9 levels	4 modes	3	101.9k	10k

- **Robustness through test-time sensor control:** We demonstrate that adjusting sensor parameters during inference under environmental variations improves 6D pose estimation accuracy by an average of 11.4% compared to standard auto-exposure with conventional digital augmentation. This indicates that sensor-level tuning can better account for the real-world variability faced during deployment. Moreover, sensor control proves to be a data-efficient approach to improving robustness, achieving comparable generalization with significantly less training data.
- **Potential of multimodal sensor adaptation:** While adapting either RGB or depth sensors individually already yields noticeable improvements, jointly optimizing both RGB and depth parameters at test-time provides even greater gains. This emphasizes the value of studying multimodal sensor interactions and highlights new directions for advancing the field of 6D pose estimation.

By providing a structured testbed for sensor-aware object 6D pose estimation, *SenseShift6D* lays the groundwork for more robust, adaptive perception systems in dynamic real-world environments.

2 Related Work

2.1 6D Pose Estimation Benchmark

Classic datasets. LineMOD (LM) [7] and its occlusion subset (LM-O) [3] pioneered RGB-D pose estimation benchmarks in controlled tabletop setups. Subsequent benchmarks such as T-LESS [10], which provided a large collection of texture-less industrial objects, and YCB-V [27], which offered cluttered scenes with temporal sequences, expanded the scope of evaluation. While these benchmarks provide robust evaluation regarding variations in objects and their poses, all were captured under fixed illumination and camera settings.

Initial exploration of environmental and sensor variation. TUD-L [11], HomebrewedDB (HB) [15], and HOPE [23] introduced variations in illumination conditions but retained fixed camera settings with auto-exposure enabled. The recent Industrial Parts Dataset (IPD) [14] was the first benchmark to vary camera parameters, capturing four exposure levels under multiple lighting conditions. However, IPD focuses on texture-less industrial parts and does not explore variations in RGB gain or depth-sensor modes, thus limiting its suitability for adaptive-sensing research.

Remaining gap and our contribution. As summarized in Table 1, no existing benchmark offers orthogonal sweeps of RGB exposure, RGB gain, and multiple depth-capture modes together with dense 6D ground truth. Our *SenseShift6D* dataset directly addresses this gap by systematically varying exposure, gain, and depth-capture modes under diverse illumination conditions, enabling fine-grained analysis of 6D pose estimation robustness to realistic hardware-level changes.

2.2 Adaptive Sensor Control Benchmark

Recent studies have explored test-time adaptation of camera sensor parameters to improve downstream vision performance. ImageNet-ES [1] and ImageNet-ES-Diverse [2] captured real-world scenes using a physical camera, systematically varying aperture, shutter speed, and ISO across multiple lighting conditions for image classification tasks. These benchmarks demonstrated that physical variation *cannot be replicated by synthetic augmentations* and dynamically selecting optimal camera parameters at test time can significantly increase the performance of lightweight models, enabling accuracy competitive with larger foundation models without additional training.

Table 2: **SenseShift6D Configurations for Data split.**

Data split	Brightness (%)	Sensor configuration	Exposure (μ s)	Gain	Depth-capture mode	Captured images
Train-Def	50	Auto (1 RGB option, 1 depth option)	Auto	Auto	Default	RGB: 385, Depth: 385 1 RGB-D scene/pose
Train-Var	5, 25, 50, 75, 100	Auto + Manual (41 RGB options, 1 depth options)	Auto, 2, 4, 19, 78, 312, 1250, 5000, 10000	Auto, 0, 32, 64, 96, 128	Default	RGB: 80.0k, Depth: 1.9k 205 RGB-D scenes/pose
Test-Def	50	Auto (1 RGB option, 1 depth option)	Auto	Auto	Default	RGB: 128, Depth: 128 1 RGB-D scenes/pose
Test-Var	5, 25, 50, 75, 100	Auto + Manual (21 RGB options, 4 Depth options)	Auto, 9, 39, 156, 625, 2500	Auto, 16, 48, 80, 112	Default, High Accuracy, High Density, Medium Density	RGB: 13k, Depth: 2.5k 420 RGB-D scenes/pose

However, existing adaptive sensing research remains limited to single-modal RGB classification. To date, no prior work has explored: (1) multimodal sensor control, where depth-sensor modes must be jointly optimized with RGB settings; or (2) the impact of adaptive sensor control on object-centric 6D pose estimation tasks, which inherently rely on both photometric and geometric cues. Our *SenseShift6D* addresses this gap by providing the first realistic testbed for evaluating multimodal, per-frame sensor-control policies alongside conventional data-centric training baselines.

3 SenseShift6D

We introduce *SenseShift6D*, the first RGB-D benchmark that *physically* sweeps camera and lighting parameters, enabling rigorous evaluation of 6D object pose estimators under realistic environmental and sensor dynamics. Using an Intel RealSense D455 mounted in a darkroom, we systematically capture three representative household objects – a textured spray can, a cylindrical Pringles tube, and a glossy tin case (Figure 3) – under auto-exposure, 13 RGB-exposure times, 9 RGB-gain settings, 4 depth-capture presets, and 5 illumination levels (details in Table 2). Our dataset consists of 101.9k RGB and 10k depth frames, which can yield 1,380 unique sensor-lighting permutations per object pose. Accurate ground truth is obtained via a rigidly mounted ChArUco board and careful hand-eye calibration.



Figure 3: **Three household objects collected in SenseShift6D.**

To facilitate controlled benchmarking, we organize the dataset into four clearly defined splits:

- **Train-Def:** Contains only the default sensor and lighting configuration (1 RGB-D scene/pose)
- **Train-Var:** Expands Train-Def, covering $(8 \text{ exposures} \times 5 \text{ gains} + 1 \text{ auto-exposure}) \times 1 \text{ depth modes} \times 5 \text{ brightness levels}$ (205 RGB-D scenes/pose).
- **Test-Def:** Includes the default sensor and lighting configuration (1 RGB-D scenes/pose)
- **Test-Var:** Expands Test-Def, featuring $(5 \text{ exposures} \times 4 \text{ gains} + 1 \text{ auto-exposure})$ configurations, spanning the same depth-mode and illumination range (420 RGB-D scenes/pose).

As all variations are physically captured rather than digitally simulated, the resulting images inherently retain authentic artifacts, such as non-linear color shifts, photon-shot noise, and depth-mode-specific errors, that synthetic augmentation methods cannot reproduce [1]. *SenseShift6D* therefore offers the first realistic testbed for analyzing environment- and sensor-aware robustness, enabling side-by-side evaluation of per-frame adaptive-sensing policies against traditional data-centric training strategies.

3.1 Environmental and Sensor Variations

Ambient-illumination sweep. Real deployments frequently encounter lighting changes, such as those found in warehouse aisles, outdoor loading bays, or dim domestic environments. To reproduce these diverse conditions in a controlled and repeatable manner, we built a darkroom enclosed with black curtains to block external light completely. Within this setup, we installed three Philips Hue White & Color Ambiance bulbs, providing precise and programmable brightness control. Each bulb was calibrated to a consistent color temperature of 6535 K, with brightness systematically varied across five levels: 5%, 25%, 50%, 75% and 100%. This controlled setting ensures uniform illumination conditions, enabling accurate comparisons of RGB gain and exposure settings under identical photon flux.

RGB-sensor parameters. The Intel RealSense D455 camera permits manual control of two key RGB sensor parameters: exposure, determining the duration of sensor exposure to incoming light, and gain, which amplifies the captured signal strength.

- **Exposure grid.** The D455 supports exposure settings ranging from $1 \mu\text{s}$ to $10,000 \mu\text{s}$. Empirical tests indicated that exposure times below $1,000 \mu\text{s}$ yield image quality comparable to the camera’s auto-exposure setting in well-lit environments. Given that this threshold is relatively low within the configurable range, we chose 13 logarithmically spaced exposure values to maximize coverage across practical operating conditions.
- **Gain grid.** The RGB gain of the D455 can be set from 0 to 128. Through visual inspection, we found that linear steps produce more diverse characteristics than exponential spacing. Therefore, we selected 9 linearly spaced gain settings spanning the full range.

Depth capture modes. The Intel RealSense D455 generates depth maps via stereo matching, estimating depth by aligning left and right camera images. This process relies on multiple internal parameters whose individual effects are complex and challenging to fine-tune directly. To manage this complexity, we leverage four predefined depth presets provided by Intel, each optimized for different usage scenarios [12]:

- **Default:** Offers visually clean depth maps with reduced noise and well-defined edges, suitable for general-purpose applications.
- **High Accuracy:** Provides highly reliable depth estimates by enforcing stricter confidence thresholds, albeit at the expense of a lower fill rate.
- **High Density:** Increases the fill factor, providing more complete depth maps, particularly effective for detecting more surfaces in low-texture areas.
- **Medium Density:** Offers a balanced trade-off between fill factor and accuracy, aiming to balance depth map completeness and precision.

3.2 Dataset Collection

To capture each scene systematically, we acquired images under all sensor configurations associated with a given data split, while maintaining fixed positions for the object and camera. Scenes were assigned exclusively to specific splits, ensuring no overlap between training and test sets. To capture diverse object poses, we used a motorized turntable to vary object orientation and adjusted the camera’s position and tilt angle. Each object was rigidly mounted onto a ChArUco board, which itself was firmly placed on the turntable, which provides a consistent and precise pose reference throughout data capture.

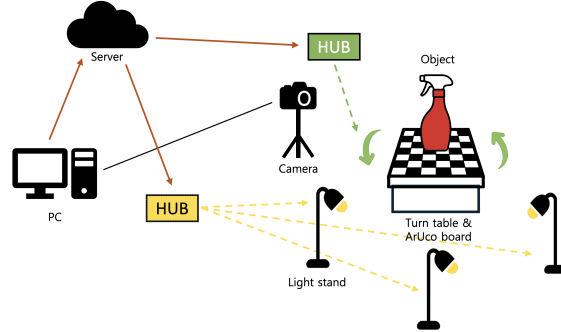


Figure 4: Testbed for data collection.

Table 3: GT annotation accuracy (mm).

	μ_δ	σ_δ	$\mu_{ \delta }$	$med_{ \delta }$
RealSense	-2.15	4.55	3.75	2.89

For automatic collection, the turntable was remotely controlled, and deliberate delays were introduced after changing lighting brightness or sensor parameters, allowing sufficient stabilization time. We employed one smart IR remote-control hub to send commands to the turntable and another hub to control three smart bulbs. Both hubs received commands from a cloud-based server, which coordinated the entire data-capture sequence through an integrated control script (see Figure 4).

3.3 Data Processing

Validation. We manually reviewed the images for each parameter configuration. If any scene appeared inconsistent due to lighting or sensor parameter change delays, we excluded that scene across all configurations to maintain dataset consistency.

Stabilizing auto-exposure frames. The default setting to capture RGB images is the auto-exposure mode. For the D455 camera, we observed that the auto-exposure setting depends on the gain value set in the previous frame, leading to frame-to-frame brightness jitter. To suppress this effect, we captured successive auto-exposure shots of each scene (5 shots for Train-Def/Var and 4 shots for Test-Def/Var), each preceded by a different gain initialization, and average them to obtain a stable reference image.

Ground-Truth annotation. For each pose, we used the 50%-brightness, averaged auto-exposure RGB frame and went through the annotation process below, resulting in 2~3 mm errors.

- **Object masks:** Initially, rough bounding boxes were generated using Grounding DINO [18], guided by shape-aware textual prompts tailored to each object. Boxes were manually reviewed and corrected if needed. The refined boxes were passed to FastSAM [29] to generate precise instance-level masks.
- **Object poses:** An initial camera-to-object transformation was provided by detecting the ChArUco markerboard rigidly attached to the turntable. The object poses were then refined precisely in 3D using the annotation utility [6] in the BOP toolkit [9] with depth maps captured in High Density mode. Finally, all refined poses were re-projected onto the RGB images and visually inspected to confirm alignment accuracy.
- **Accuracy of GT annotation:** Following the protocol in [10, 15], we calculate the difference $\delta = d_c - d_r$, where d_c denotes the captured depth map and d_r denotes the rendered depth map using the GT pose. Differences over 5 cm are treated as outliers and omitted. Table 3 reports the mean μ_δ , standard deviation σ_δ , and the mean and median of the absolute differences $\mu_{|\delta|}$ and $med_{|\delta|}$. High-accuracy depth sensing is employed for reliable evaluation of GT accuracy analysis.

4 Experiments

To assess how sensor control improves efficiency in 6D pose estimation relative to conventional training and inference approaches, we conducted experiments on several state-of-the-art models.

4.1 Experiment Setup

Models. We chose three 6D object pose estimation models: ZebraPose [22], GDRNPP [19], and HiPose [17]. ZebraPose is an RGB-based method that leverages features extracted from a ResNet-34 backbone. GDRNPP improves upon its predecessor, GDR-Net [25], by adopting a ConvNeXt [20] backbone and modifying training details such as learning rate scheduling and weight decay. While GDRNPP includes a depth-based pose refinement module, its inference primarily relies on RGB inputs. HiPose is an RGB-D model that uses ConvNeXt as the RGB backbone and RandLA-Net [13] to extract point cloud features from depth. These RGB and depth features are fused through a bidirectional interaction module for pose estimation. In our experiments, we excluded the refinement stage for ZebraPose and GDRNPP, while evaluating the full pipeline of HiPose.

Train setup. For training, we first generated 10k photorealistic (PBR) synthetic images per object using BlenderProc [4]. Each model was trained independently on a per-object basis, following one of the three schemes: (1) **PBR + Train-Def** (default physical images only), (2) **PBR + Train-Def with data augmentation** (including Gaussian blur, linear contrast adjustment, brightness enhancement and others – see Appendix A for details), and (3) **PBR + Train-Var** (full sensor and lighting variation). ZebraPose and GDRNPP were trained using an NVIDIA RTX 3090 GPU, while HiPose was trained on an NVIDIA A100 GPU. During training, we utilized depth images captured under the default-capture mode.

Metric. We used the standard Average Distance (ADD) metric [8] to evaluate model performance. ADD measures the average point-wise distance between model points transformed by the predicted pose and the ground-truth pose:

$$\text{ADD} = \frac{1}{m} \sum_{\mathbf{x} \in \mathcal{M}} \left\| (\mathbf{R}\mathbf{x} + \mathbf{T}) - (\tilde{\mathbf{R}}\mathbf{x} + \tilde{\mathbf{T}}) \right\|, \quad (1)$$

where \mathcal{M} denotes the set of 3D model points, $\mathbf{x} \in \mathcal{M}$ represents an individual point on the model, m is the total number of points in the model. \mathbf{R} and \mathbf{T} are the ground-truth rotation matrix and translation vector, while $\tilde{\mathbf{R}}$ and $\tilde{\mathbf{T}}$ are their predicted counterparts.

4.2 Analysis on RGB Sensor Control

Table 4 evaluates the impact of illumination and RGB sensor variations on 6D pose estimation. All reported results utilize the ADD metric, using AR@5, which corresponds to recall at a threshold of 5% of the object diameter. We compare three sensor control settings: (1) **AE** (auto-exposure)

Table 4: **Performance of various sensor control methods under different training and test settings of *SenseShift6D*.**

Object	Train	ZebraPose [22]				GDRNPP [19]				HiPose [17]			
		Test-Def		Test-Var		Test-Def		Test-Var		Test-Def		Test-Var	
		AE	AE	Rand	Oracle	AE	AE	Rand	Oracle	AE	AE	Rand	Oracle
Spray	PBR + Train-Def	100.0	96.09	52.26	99.51	100.0	96.59	52.02	99.02	100.0	98.73	60.00	100.0
	PBR + Train-Def w/ Aug	100.0	98.04	68.46	100.0	100.0	98.54	71.88	100.0	100.0	100.0	89.61	100.0
	PBR + Train-Var	97.56	97.07	78.80	97.56	97.56	97.56	85.93	98.54	100.0	100.0	100.0	100.0
Pringles	PBR + Train-Def	85.71	75.71	38.87	94.75	69.05	60.95	35.64	89.05	100.0	96.00	58.74	100.0
	PBR + Train-Def w/ Aug	73.80	66.18	40.92	89.99	80.95	79.05	49.17	89.52	97.62	97.81	72.81	100.0
	PBR + Train-Var	90.47	89.04	68.35	95.23	90.48	90.004	72.22	97.14	97.62	97.62	86.86	98.10
Tincase	PBR + Train-Def	95.55	84.43	44.15	96.00	82.22	75.11	43.29	90.67	73.33	60.36	40.27	77.78
	PBR + Train-Def w/ Aug	95.55	88.88	53.37	99.10	73.33	69.78	48.85	94.67	75.56	72.44	51.09	76.00
	PBR + Train-Var	97.77	96.88	73.55	99.55	95.56	95.11	77.05	97.78	75.56	73.87	73.09	75.11
Overall	PBR + Train-Def	93.75	85.41	45.09	96.75	72.60	77.53	43.65	92.91	91.11	85.03	53.00	92.59
	PBR + Train-Def w/ Aug	89.78	84.37	54.25	96.36	79.20	82.45	56.63	94.73	91.06	90.08	71.17	92.00
	PBR + Train-Var	95.26	94.33	73.56	97.44	94.53	94.23	78.40	97.82	91.06	90.50	86.65	91.07

represents the conventional baseline with automatic sensor settings; (2) **Rand** (random exposure and gain) indicates average performance across randomly selected sensor configurations; (3) **Oracle** represents the best achievable performance through optimal sensor control – measuring the probability that at least one sensor-controlled configuration enables correct pose prediction for a given scene.

In Table 4, AE consistently exhibits lower performance on Test-Var compared to Test-Def (captured at the same 50% brightness level as Train-Def), regardless of the model or training strategy. This clearly illustrates the necessity of evaluating model robustness under realistic illumination shifts. Applying digital augmentation during training generally improves AE performance on Test-Var, yet adversely affects certain cases (e.g., ZebraPose for Pringles and GDRNPP for Tincase), suggesting that augmentation alone may not reliably enhance robustness. In contrast, training models on physically collected data (Train-Var, which is 3.5 times larger than Train-Def) consistently yields greater performance gains compared to digital augmentation, highlighting the inherent limitations of synthetic simulation in accurately replicating real-world environmental variations. Given that physically collecting large-scale, diverse datasets is often challenging in practice, this performance gap underscores the need for an efficient test-time adaptation methods to effectively address sensor and environmental shifts.

Model-friendly sensor control vs. Traditional auto-exposure. Within Test-Var, AE significantly outperforms Rand, showing the critical role of intentional sensor control in managing environmental variability. Furthermore, Oracle consistently surpasses AE across all models and training strategies, verifying that the auto-exposure mechanism – typically optimized for human visual perception – is not necessarily optimal for model performance. Thus, substantial potential exists for model-specific sensor adaptation at test time, without modifying model architectures or training schemes. Notably, Oracle achieves over 13.4% average performance improvement compared to AE for RGB-based models (ZebraPose and GDRNPP).

Test-time sensor control vs. Traditional generalization approaches. Oracle without augmentation (i.e., the first training scheme) consistently surpasses AE with augmentation, and even outperforms AE trained on Train-Var in most scenarios. In the worst case (GDRNPP), Oracle trained on Train-Def remains comparable to AE trained on Train-Var, showing less than a 2% accuracy gap. These superior results, relative to traditional generalization strategies, such as augmentation or manual scaling training data, demonstrate the substantial potential of test-time sensor control for 6D pose estimation in dynamic real-world environments. Consequently, mitigating covariate shifts during inference through sensor optimization may be more effective, or complementary, compared to exclusively focusing on model generalization to all possible covariate variations, as currently pursued by foundational-model approaches.

4.3 Analysis on Multimodal RGB-D Sensor Control

To comprehensively analyze the impact of multimodal sensor control under environmental variations, we train HiPose (an RGB-D model) following the first training scheme (PBR + Train-Def, captured at 50% brightness level) and evaluate it on the Test-Var split. To specifically assess high-precision pose estimation, we report AUC@[0:0.1], which measures the area under the ADD recall curve within 10% of the object diameter. We consider five conditions: (1) **Baseline** utilizes the default settings

Table 5: AUC performance of various sensor control methods for HiPose, trained on PBR + Train-Def and tested on Test-Var.

Object	Baseline	Depth-Only	RGB-Only	Oracle-Fixed	Oracle-Dynamic
	RGB: Auto Depth: Default	RGB: Auto Depth: Oracle	RGB: Oracle Depth: Default	Best Fixed Param.	RGB: Oracle Depth: Oracle
Spray	86.80	88.04(+1.24)	88.87(+2.07)	86.80	89.92(+3.12)
Pringles	73.65	76.10(+2.45)	78.92(+5.27)	74.68(+1.03)	81.42(+7.77)
Tincase	56.07	58.63(+2.56)	63.60(+7.53)	56.10(+0.03)	66.92 (+10.85)
Overall	72.17	74.25(+2.08)	77.13(+4.95)	72.53(+0.53)	79.42(+7.24)

for both RGB and depth sensors; (2) **Depth-Only** applies Oracle selection for the depth sensor, while maintaining auto-exposure settings for RGB; (3) **RGB-Only** applies Oracle selection for the RGB sensor, while using the Default mode for the depth sensor; (4) **Oracle-Fixed** selects the single best-performing fixed RGB-D configuration and applies it across all test scenes; (5) **Oracle-Dynamic** applies Oracle selection to both RGB and depth sensors for each scene.

Table 5 shows that all four sensor-control methods outperform Baseline across every scenario. Among these methods, Oracle-Fixed yields the smallest improvement, offering only marginal gains over Baseline despite controlling multimodal sensor parameters. This result highlights the impracticality of relying on a single, fixed sensor configuration to handle diverse environmental variations; instead, sensor parameters must be adapted dynamically on a per-scene basis.

Complementary role of RGB and Depth. Interestingly, Depth-Only achieves a notable AUC improvement of 2.08% compared to Baseline, demonstrating consistent benefits across all objects. Even though the model was trained exclusively with the Default depth-capture mode – suggesting that employing alternative modes at inference might introduce covariate shifts – allowing flexible depth-mode selection still substantially enhances pose estimation performance. RGB-Only further improves performance relative to Depth-Only, particularly for symmetric objects (Pringles and Tincase). This suggests that RGB surface information may provide crucial cues for accurately estimating the poses of symmetric objects.

Multimodal joint control vs. Unimodal control. Oracle-Dynamic achieves the best overall performance, improving AUC by 7.24% over Baseline and by 2.95% over the second-best RGB-Only method. Notably, Oracle-Dynamic exhibits the most significant gain for Tincase (10.85% above Baseline), the most challenging object in our dataset. These results indicate that RGB and depth modalities provide complementary information, and that jointly adapting both sensors creates synergy exceeding that achievable by independently adapting individual modalities. Thus, our findings highlight the importance of deeper investigations into multimodal sensor adaptation strategies and understanding which combinations of RGB-D inputs are most beneficial for model performance.

4.4 Qualitative Analysis

Analysis on RGB sensor control. Figure 5 illustrates two representative test scenes for GDRNPP, involving the Tincase and Pringles objects, respectively. In both cases, AE results in incorrect pose predictions (via GDRNPP), while Oracle (RGB-only) successfully estimates accurate object poses. These scenes were captured at the lowest brightness level, representing the most challenging environmental condition. These examples highlight that optimal RGB sensor parameters, especially gain values in these cases, vary depending on both object type and object pose, underscoring the necessity of per-scene test-time sensor control. Furthermore, the RGB images selected by Oracle and AE appear visually indistinguishable from a human perspective. This indicates that the optimal direction for model-friendly sensor control is not always intuitively aligned with human visual perception, emphasizing the importance of sensor control strategies specifically tailored to model performance rather than subjective human assessment.

Analysis on depth sensor control. Figure 6 illustrates two representative test scenes evaluated with HiPose, involving the Tincase and Pringles objects, respectively. Both scenes were captured at the lowest brightness level, representing the most challenging environmental conditions. While the RGB sensor parameters were fixed, we compared pose estimation performance across different depth-capture modes. In both cases, the Default depth mode resulted in incorrect pose predictions,

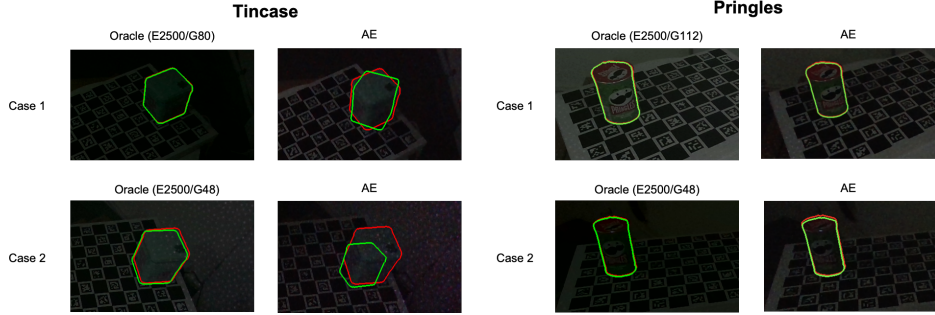


Figure 5: **RGB visualization of pose estimation results under auto exposure and sensor control settings.** The red line represents the ground truth pose, and the green line indicates the predicted pose.

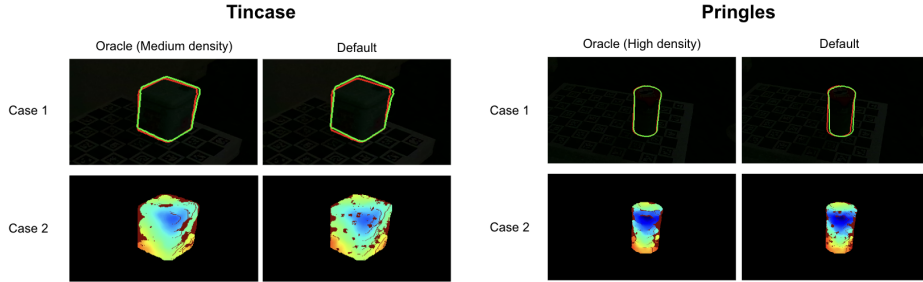


Figure 6: **Visualization of pose estimation results showing that depth modes other than the default yield better performance under a fixed RGB configuration (E2500, G16).** Red lines denote ground truth poses, while green lines represent predicted poses.

whereas Oracle (Depth-only) successfully produced accurate object poses. These examples clearly demonstrate that different depth-capture modes yield varying depth-map qualities, affecting pose estimation outcomes. Furthermore, the optimal depth-capture mode depends on the specific object type and scene configuration, underscoring the importance of adaptive, scene-dependent depth-sensor control strategies.

5 Conclusion

We introduced *SenseShift6D*, the first sensor-aware, multimodal benchmark for 6D object-pose estimation that *physically* sweeps RGB exposure, RGB gain, depth-capture mode, and ambient illumination. Extensive experiments show that state-of-the-art methods suffer substantial accuracy drops under these realistic sensor shifts. Crucially, we demonstrated that adaptive sensor control at test time can recover a large portion of this lost performance – without any model retraining – and that joint RGB + depth control outperforms unimodal strategies. These findings highlight sensor control as a promising and lightweight avenue for deploying 6D-pose systems in dynamic, real-world conditions.

Limitations and Future Work. *SenseShift6D* currently focuses on single-object tabletop scenes and varies only brightness intensity, omitting complexities such as directional lighting, shadows, and occlusions. Future extensions of the dataset will include: (1) multi-object scenarios to explore occlusion and clutter; (2) directional and shadow-rich lighting conditions; and (3) a real-time adaptive sensor-control framework that dynamically adjusts RGB and depth parameters. We believe *SenseShift6D* provides a strong foundation for developing robust, sensor-adaptive 6D pose estimation systems suitable for deployment in diverse and dynamic real-world environments.

References

- [1] Eunsu Baek, Keondo Park, Jiyeon Kim, and Hyung-Sin Kim. Unexplored faces of robustness and out-of-distribution: Covariate shifts in environment and sensor domains. In *Proceedings of the IEEE/CVF Conference on Computer Vision and Pattern Recognition*, pages 22294–22303, 2024.
- [2] Eunsu Baek, Sunghwan Han, Taesik Gong, and Hyung-Sin Kim. Adaptive camera sensor for vision models. In *The Thirteenth International Conference on Learning Representations*, 2025.
- [3] Eric Brachmann, Alexander Krull, Frank Michel, Stefan Gumhold, Jamie Shotton, and Carsten Rother. Learning 6d object pose estimation using 3d object coordinates. In *Computer Vision—ECCV 2014: 13th European Conference, Zurich, Switzerland, September 6–12, 2014, Proceedings, Part II 13*, pages 536–551. Springer, 2014.
- [4] Maximilian Denninger, Dominik Winkelbauer, Martin Sundermeyer, Wout Boerdijk, Markus Knauer, Klaus H. Strobl, Matthias Humt, and Rudolph Triebel. Blenderproc2: A procedural pipeline for photorealistic rendering. *Journal of Open Source Software*, 8(82):4901, 2023. doi: 10.21105/joss.04901. URL <https://doi.org/10.21105/joss.04901>.
- [5] Mitchell Doughty and Nilesh R Ghugre. Hmd-egopose: Head-mounted display-based egocentric marker-less tool and hand pose estimation for augmented surgical guidance. *International journal of computer assisted radiology and surgery*, 17(12):2253–2262, 2022.
- [6] Anas Gouda, Abraham Ghanem, and Christopher Reining. Dopose-6d dataset for object segmentation and 6d pose estimation. In *2022 21st IEEE International Conference on Machine Learning and Applications (ICMLA)*, pages 477–483. IEEE, 2022.
- [7] Stefan Hinterstoisser, Vincent Lepetit, Slobodan Ilic, Stefan Holzer, Gary Bradski, Kurt Konolige, and Nassir Navab. Model based training, detection and pose estimation of texture-less 3d objects in heavily cluttered scenes. In *Asian conference on computer vision*, pages 548–562. Springer, 2012.
- [8] Stefan Hinterstoisser, Vincent Lepetit, Slobodan Ilic, Stefan Holzer, Gary Bradski, Kurt Konolige, and Nassir Navab. Model based training, detection and pose estimation of texture-less 3d objects in heavily cluttered scenes. In *Asian conference on computer vision*, pages 548–562. Springer, 2012.
- [9] Tomas Hodan and Martin Sundermeyer. BOP Toolkit. https://github.com/thodan/bop_toolkit, 2020.
- [10] Tomáš Hodan, Pavel Haluza, Štěpán Obdržálek, Jiri Matas, Manolis Lourakis, and Xenophon Zabulis. T-less: An rgb-d dataset for 6d pose estimation of texture-less objects. In *2017 IEEE Winter Conference on Applications of Computer Vision (WACV)*, pages 880–888. IEEE, 2017.
- [11] Tomas Hodan, Frank Michel, Eric Brachmann, Wadim Kehl, Anders GlentBuch, Dirk Kraft, Bertram Drost, Joel Vidal, Stephan Ihrke, Xenophon Zabulis, et al. Bop: Benchmark for 6d object pose estimation. In *Proceedings of the European conference on computer vision (ECCV)*, pages 19–34, 2018.
- [12] Yusheng Hsu, Anders Grunnet-Jepsen, John Sweetser, and Shirit Brook. D400 series visual presets, 2023. URL <https://dev.intelrealsense.com/docs/d400-series-visual-presets>. Accessed: May 12, 2025.
- [13] Qingyong Hu, Bo Yang, Linhai Xie, Stefano Rosa, Yulan Guo, Zhihua Wang, Niki Trigoni, and Andrew Markham. Randla-net: Efficient semantic segmentation of large-scale point clouds. In *Proceedings of the IEEE/CVF conference on computer vision and pattern recognition*, pages 11108–11117, 2020.
- [14] Agastya Kalra, Guy Stoppi, Dmitrii Marin, Vage Taamazyan, Aarrushi Shandilya, Rishav Agarwal, Anton Boykov, Tze Hao Chong, and Michael Stark. Towards co-evaluation of cameras hdr and algorithms for industrial-grade 6dof pose estimation. In *Proceedings of the IEEE/CVF Conference on Computer Vision and Pattern Recognition*, pages 22691–22701, 2024.

- [15] Roman Kaskman, Sergey Zakharov, Ivan Shugurov, and Slobodan Ilic. Homebreweddb: Rgb-d dataset for 6d pose estimation of 3d objects. In *Proceedings of the IEEE/CVF International Conference on Computer Vision Workshops*, pages 0–0, 2019.
- [16] Lei Ke, Shichao Li, Yanan Sun, Yu-Wing Tai, and Chi-Keung Tang. Gsnet: Joint vehicle pose and shape reconstruction with geometrical and scene-aware supervision. In *Computer Vision—ECCV 2020: 16th European Conference, Glasgow, UK, August 23–28, 2020, Proceedings, Part XV 16*, pages 515–532. Springer, 2020.
- [17] Yongliang Lin, Yongzhi Su, Praveen Nathan, Sandeep Inuganti, Yan Di, Martin Sundermeyer, Fabian Manhardt, Didier Stricker, Jason Rambach, and Yu Zhang. Hipose: Hierarchical binary surface encoding and correspondence pruning for rgb-d 6dof object pose estimation. In *Proceedings of the IEEE/CVF Conference on Computer Vision and Pattern Recognition*, pages 10148–10158, 2024.
- [18] Shilong Liu, Zhaoyang Zeng, Tianhe Ren, Feng Li, Hao Zhang, Jie Yang, Qing Jiang, Chunyuan Li, Jianwei Yang, Hang Su, et al. Grounding dino: Marrying dino with grounded pre-training for open-set object detection. In *European Conference on Computer Vision*, pages 38–55. Springer, 2024.
- [19] Xingyu Liu, Ruida Zhang, Chenyangguang Zhang, Gu Wang, Jiwen Tang, Zhigang Li, and Xiangyang Ji. Gdrnpp: A geometry-guided and fully learning-based object pose estimator. *IEEE Transactions on Pattern Analysis and Machine Intelligence*, 2025.
- [20] Zhuang Liu, Hanzi Mao, Chao-Yuan Wu, Christoph Feichtenhofer, Trevor Darrell, and Saining Xie. A convnet for the 2020s. In *Proceedings of the IEEE/CVF conference on computer vision and pattern recognition*, pages 11976–11986, 2022.
- [21] Georgy Ponimatkin, Martin Cífka, Tomáš Souček, Médéric Fourmy, Yann Labbé, Vladimir Petrik, and Josef Sivic. 6D Object Pose Tracking in Internet Videos for Robotic Manipulation. In *The Thirteenth International Conference on Learning Representations*, 2025.
- [22] Yongzhi Su, Mahdi Saleh, Torben Fetzner, Jason Rambach, Nassir Navab, Benjamin Busam, Didier Stricker, and Federico Tombari. Zebrapose: Coarse to fine surface encoding for 6dof object pose estimation. In *Proceedings of the IEEE/CVF Conference on Computer Vision and Pattern Recognition*, pages 6738–6748, 2022.
- [23] Martin Sundermeyer, Tomas Hodan, Bertram Drost, Suat Gedikli, David Winkelbauer, Zoltan-Csaba Marton, Matthias Brucker, Nicolas Zeller, and Rudolph Triebel. Hope: A household objects dataset for pose estimation. In *Proceedings of the IEEE/RSJ International Conference on Intelligent Robots and Systems (IROS)*, pages 9664–9671, 2022.
- [24] Michał Trojak, Artur Jurgas, Maciej Stanuch, Łukasz Kownacki, and Andrzej Skalski. Mixed reality 6d object pose estimation using deep learning for visual markerless surgical navigation. In *2025 IEEE Conference on Virtual Reality and 3D User Interfaces Abstracts and Workshops (VRW)*, pages 947–952. IEEE, 2025.
- [25] Gu Wang, Fabian Manhardt, Federico Tombari, and Xiangyang Ji. Gdr-net: Geometry-guided direct regression network for monocular 6d object pose estimation. In *Proceedings of the IEEE/CVF Conference on Computer Vision and Pattern Recognition*, pages 16611–16621, 2021.
- [26] Di Wu, Zhaoyong Zhuang, Canqun Xiang, Wenbin Zou, and Xia Li. 6d-vnet: End-to-end 6-dof vehicle pose estimation from monocular rgb images. In *Proceedings of the IEEE/CVF Conference on Computer Vision and Pattern Recognition Workshops*, pages 0–0, 2019.
- [27] Yu Xiang, Tanner Schmidt, Venkatraman Narayanan, and Dieter Fox. Posecnn: A convolutional neural network for 6d object pose estimation in cluttered scenes. *arXiv preprint arXiv:1711.00199*, 2017.
- [28] Chengjie Zhang, Chengyu Lin, Yuquan Leng, Zezheng Fu, Yaoyu Cheng, and Chenglong Fu. An effective head-based hri for 6d robotic grasping using mixed reality. *IEEE Robotics and Automation Letters*, 8(5):2796–2803, 2023.

- [29] Xu Zhao, Wenchao Ding, Yongqi An, Yinglong Du, Tao Yu, Min Li, Ming Tang, and Jinqiao Wang. Fast segment anything. *arXiv preprint arXiv:2306.12156*, 2023.

Appendix

A RGB Augmentation Settings

To improve generalization under varying environmental conditions, we adopted an RGB augmentation pipeline based on that used in GDRNPP. The augmentations were implemented using the `imgaug` library and applied only to the RGB input during training with a probability of 0.8. An overview of these augmentations is illustrated in Figure 7.

The augmentations listed in Table 6 were applied in random order, with each operation activated independently with a fixed probability.

Table 6: Augmentation operations and parameters.

Augmentation Type	Activation Probability	Parameters / Range
Gaussian Blur	0.4	$\sigma \in [0.0, 3.0]$
Sharpness Enhancement	0.3	factor $\in [0.0, 50.0]$
Contrast Enhancement	0.3	factor $\in [0.2, 50.0]$
Brightness Enhancement	0.5	factor $\in [0.1, 6.0]$
Color Enhancement	0.3	factor $\in [0.0, 20.0]$
Additive Intensity	0.5	value $\in [-25, 25]$, per-channel = 0.3
Invert Pixels	0.3	probability = 0.2, per-channel
Multiply Intensity	0.5	factor $\in [0.6, 1.4]$, per-channel = 0.5
Additive Gaussian Noise	0.1	scale = 10, per-channel
Linear Contrast	0.5	factor $\in [0.5, 2.2]$, per-channel = 0.3
Grayscale Conversion	0.5	$\alpha \in [0.0, 1.0]$

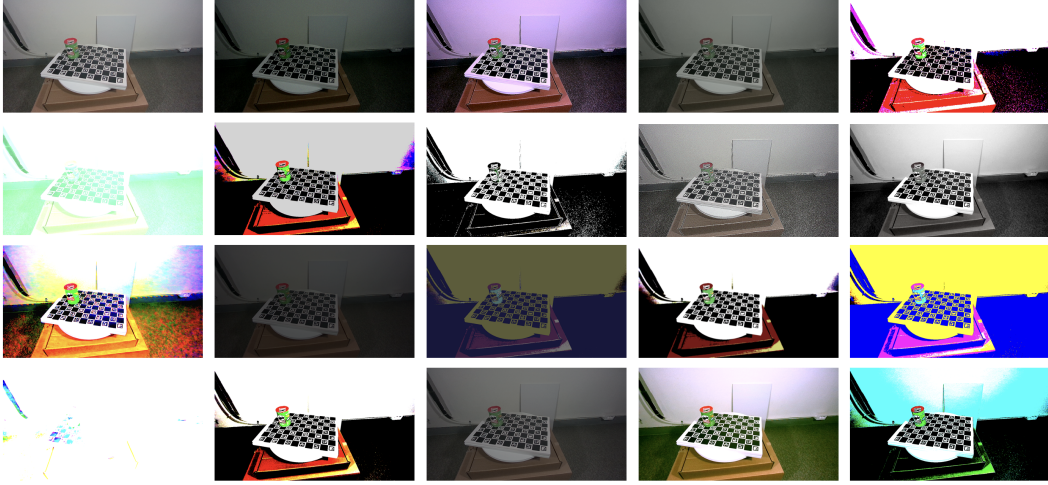


Figure 7: **Examples of RGB augmentations applied during training.** The top-left image is the original, and the remaining images are randomly augmented samples generated using the settings summarized in Table 6.

B Licenses

We use open-source components under various licenses for evaluation and data generation. In particular, some scripts for photorealistic rendering are adapted from *BlenderProc* (GPL-3.0), and evaluation pipelines integrate components from *GDRNPP* (Apache-2.0), *ZebraPose* (MIT), and *HiPose* (MIT). All third-party code is used in compliance with their respective licenses, with attribution provided as required.

Our dataset, *SenseShift6D*, is distributed under the **Creative Commons Attribution 4.0 International (CC BY 4.0)** license.

C Experimental Details

C.1 Compute Resources

All models were trained on a high-performance computing cluster equipped with NVIDIA GPUs and Intel Xeon CPUs. Specifically, *ZebraPose* and *GDRNPP* were trained on nodes with RTX 3090 GPUs (24GB VRAM) and Intel Xeon Silver 4210R CPUs, while *HiPose* was trained on a node with A100 GPUs (80GB VRAM) and an Intel Xeon Gold 6530 CPU. Each training node had access to 512GB of RAM.

C.2 Model Training

All models were trained with a batch size of 32. *ZebraPose* and *HiPose* were both trained for a total of 38,000 iterations using the Adam optimizer, with learning rates of 0.0002 and 0.0001, respectively. *GDRNPP* was trained for 120 epochs using the Ranger optimizer with a learning rate of 8e-4 and weight decay of 0.01. A flat-and-anneal learning rate schedule with cosine annealing was applied, starting at 72% of the total training epochs. A linear warmup was used for the first 1,000 iterations with a warmup factor of 0.001. All learning rate schedules and optimizer settings follow the original implementations of each method.

Table 7: Configurations for various data split.

Data split	Brightness (%)	Sensor configuration	Exposure (μ s)	Gain	Depth-capture mode
Train-B5Def	5	Auto (1 RGB option, 1 depth option)	Auto	Auto	Default
Train-BADef	5, 25, 50, 75, 100	Auto (1 RGB option, 1 depth option)	Auto	Auto	Default
Train-B50Var	50	Auto + Manual (41 RGB options, 1 depth options)	Auto, 2, 4, 19, 78, 312, 1250, 5000, 10000	Auto, 0, 32, 64, 96, 128	Default
Test-B5Def	5	Auto (1 RGB option, 1 depth option)	Auto	Auto	Default, High Accuracy, High Density, Medium Density
Test-B5Var	5	Auto + Manual (21 RGB options, 4 Depth options)	Auto, 9, 39, 156, 625, 2500	Auto, 16, 48, 80, 112	Default, High Accuracy, High Density, Medium Density

D Additional Evaluation Results

Table 8 presents the performance of the Tincase in Table 4, categorized by brightness level. This suggests a noticeable difference in performance at brightness 5 compared to other brightness levels. Therefore, we evaluated *SenseShift6D* dataset on various data splits, beyond those described in Table 2. Each split is detailed in Table 7.

D.1 Trained without Environmental Shift

We conducted an experiment under the low-light condition of brightness 5, which yielded the lowest performance in brightness-wise evaluation. To eliminate environmental shifts, we set both training and testing to brightness 5, replacing the default training condition (brightness 50). As shown in Table 9, the oracle with sensor control achieves performance comparable to or even better than training and testing conducted entirely within the same brightness 5 domain, suggesting that adaptive sensor control can mitigate domain gaps without the need for retraining in the target environment.

Table 8: Performance of sensor control across brightness levels for Tincase.

Brightness	Test-Var	ZebraPose			GDRNPP			HiPose		
		PBR+ Train-Def	PBR+ Train-Def w/ Aug	PBR+ Train-Var	PBR+ Train-Def	PBR+ Train-Def w/ Aug	PBR+ Train-Var	PBR+ Train-Def	PBR+ Train-Def w/ Aug	PBR+ Train-Var
B5	AE	33.33	64.44	95.55	37.78	40.00	93.33	10.67	64.89	71.56
	Rand	9.67	15.56	36.89	13.56	19.44	42.55	10.78	18.67	69.11
	Oracle	80.00	97.78	97.78	88.89	91.11	100.00	75.56	71.11	71.11
B25	AE	97.78	93.33	95.56	84.44	73.33	95.56	71.11	73.33	73.33
	Rand	46.11	51.11	70.00	43.89	46.22	75.11	38.67	44.56	73.33
	Oracle	100.00	97.78	100.00	91.11	95.56	97.78	77.78	73.33	73.33
B50	AE	95.56	95.56	97.78	82.22	75.56	95.56	72.44	75.11	73.78
	Rand	56.11	64.67	87.00	55.33	58.00	88.34	53.00	60.89	73.56
	Oracle	100.00	100.00	100.00	91.11	97.78	97.78	77.78	77.78	75.56
B75	AE	97.78	93.33	97.78	84.44	80.00	95.56	73.78	74.22	76.44
	Rand	54.22	69.44	89.78	50.22	62.78	92.11	46.78	69.44	75.33
	Oracle	100.00	100.00	100.00	91.11	95.56	97.78	80.00	80.00	77.78
B100	AE	97.78	97.78	97.78	86.67	80.00	95.56	73.78	74.67	74.22
	Rand	54.67	66.11	84.11	53.45	57.78	87.11	52.11	61.89	74.11
	Oracle	100.00	100.00	100.00	91.11	93.33	95.56	77.78	77.78	77.78
Overall	AE	84.43	88.88	96.88	75.11	69.78	95.11	60.36	72.44	73.87
	Rand	44.15	53.37	73.55	42.29	48.85	77.05	40.27	51.09	73.09
	Oracle	96.00	99.10	99.55	90.67	94.67	97.78	77.78	76.00	75.11

Table 9: Comparison of models trained without environmental shift under brightness 5.

Model	Train-B5Def		Train-Def	
	Test-B5Def	Test-B5Def	Test-B5Var	Test-B5Var
	AE	AE	Rand	Oracle
ZebraPose	26.66	33.33	9.66	80.00
GDRNPP	86.67	37.78	13.56	88.89
HiPose	35.44	10.67	10.78	75.56

D.2 Trained on Diverse Sensor and Environmental Settings

In contrast to Train-Var, we partially incorporated sensor control and environmental variability into the training process. Table 10 presents AUC performance at [0:0.1], indicating that including sensor-controlled images at a fixed brightness level (Train-B50Var) can lead to improved generalization across diverse environmental conditions, when compared to using auto exposure images from multiple brightness levels (Train-BADef). This indicates that sensor control introduces rich variations which act as implicit regularization against domain shifts. Notably, even without additional training, appropriate sensor configuration at test time contributes significantly to model performance, as shown by the oracle performance under the Train-Def setting.

Table 10: AUC performance under various brightness and sensor configurations for Tincase.

Train	ZebraPose				GDRNPP				HiPose			
	Test-Def		Test-Var		Test-Def		Test-Var		Test-Def		Test-Var	
	AE	AE	Rand	Oracle	AE	AE	Rand	Oracle	AE	AE	Rand	Oracle
Train-Def	76.80	68.14	38.20	84.62	67.34	60.93	31.51	77.50	61.58	55.90	34.78	64.22
Train-BADef	78.73	70.09	37.31	83.96	81.54	80.38	48.83	89.04	61.82	55.36	34.32	63.73
Train-B50Var	78.91	77.00	56.16	85.58	81.17	79.69	62.03	87.48	61.82	61.54	60.47	63.00
Train-Var	80.44	79.54	61.91	86.60	79.32	78.64	64.20	85.46	61.73	61.61	60.86	63.13

E Additional Qualitative Results on Depth Variations

Figure 8 visualizes how the object region appears in the depth map under each depth capture mode for all three objects. In addition, Figure 9 shows qualitative examples for Tincase, using HiPose trained on Train-Def. Given a fixed RGB image with poor visibility, the figure compares predictions and corresponding masked depth maps between the default mode and oracle-selected modes, where the

default mode fails across all examples while the oracle modes often produce better results including some successful predictions.

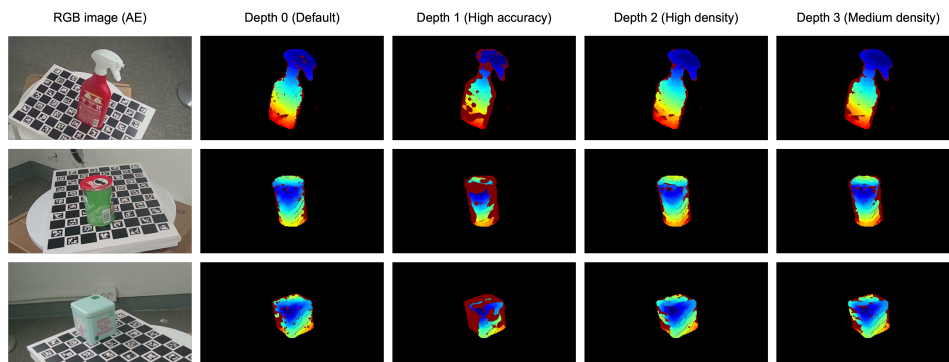


Figure 8: Visualization of masked object depth maps across different capture modes.

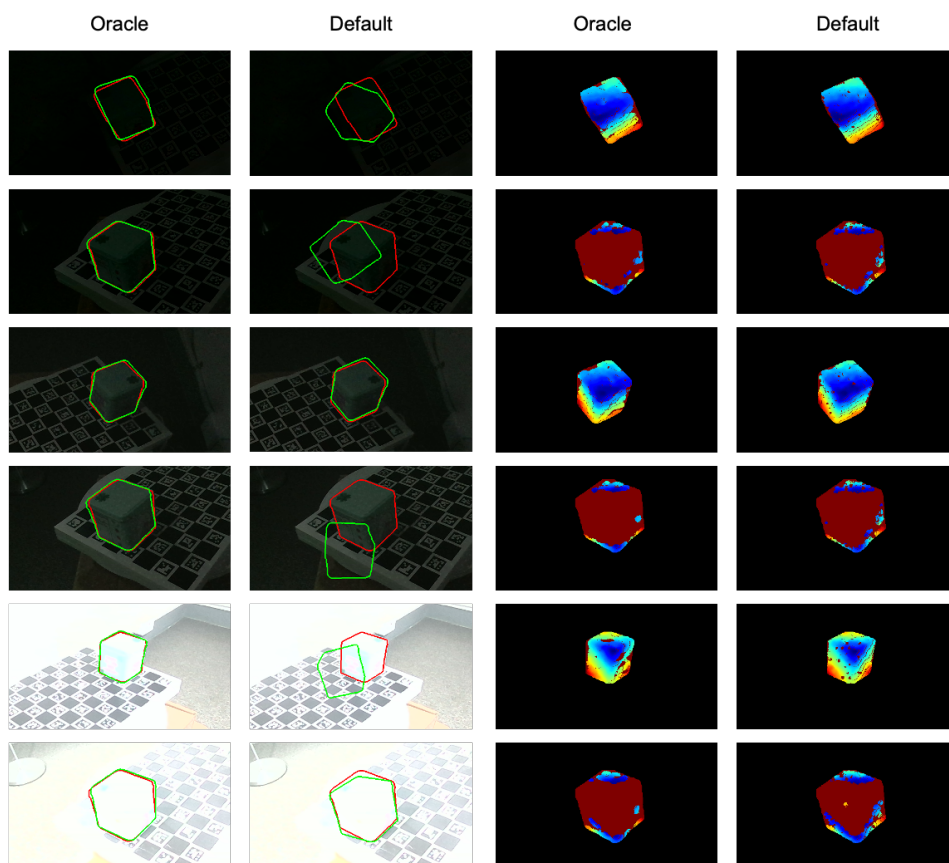


Figure 9: Comparison of predictions under default and oracle capture modes with a fixed RGB image. (Left) Visualized object pose on RGB images: ground truth pose in red, predicted pose in green. (Right) Masked depth maps corresponding to each capture mode.